

Diffusion Bonding of 17-4 Precipitation Hardening Stainless Steel to Ti Alloy With and Without Ni Alloy Interlayer: Interface Microstructure and Mechanical Properties

S. KUNDU, G. ANAND, and S. CHATTERJEE

In the present study, the diffusion bonding of 17-4 precipitation hardening stainless steel to Ti alloy with and without nickel alloy as intermediate material was carried out in the temperature range of 1073 K to 1223 K (800 °C to 950 °C) in steps of 298 K (25 °C) for 60 minutes in vacuum. The effects of bonding temperature on interfaces microstructures of bonded joint were analyzed by light optical and scanning electron microscopy. In the case of directly bonded stainless steel and titanium alloy, the layerwise α -Fe + χ , χ , FeTi + λ , FeTi + β -Ti phase, and phase mixture were observed at the bond interface. However, when nickel alloy was used as an interlayer, the interfaces indicate that Ni₃Ti, NiTi, and NiTi₂ are formed at the nickel alloy-titanium alloy interface and the PHSS-nickel alloy interface is free from intermetallics up to 1148 K (875 °C) and above this temperature, intermetallics were formed. The irregular-shaped particles of Fe₅Cr₃₅Ni₄₀Ti₁₅ have been observed within the Ni₃Ti intermetallic layer. The joint tensile and shear strength were measured; a maximum tensile strength of ~477 MPa and shear strength of ~356.9 MPa along with ~4.2 pct elongation were obtained for the direct bonded joint when processed at 1173 K (900 °C). However, when nickel base alloy was used as an interlayer in the same materials at the bonding temperature of 1148 K (875 °C), the bond tensile and shear strengths increase to ~523.6 and ~389.6 MPa, respectively, along with 6.2 pct elongation.

DOI: 10.1007/s11661-012-1553-2

© The Minerals, Metals & Materials Society and ASM International 2012

I. INTRODUCTION

THE dissimilar material joint of Ti alloy and precipitation hardening stainless steel (PHSS) is potentially applied for attractive products for various applications. For instance, a golf club head can be made by a Ti alloy striking plate and a PHSS body.^[1,2] The conventional fusion welding method is not suitable for joining them due to a high possibility of the brittle intermetallics formation in the weld zone, in addition to the difference in melting points of these two materials. Furthermore, Ti alloy and stainless steel have wide differences in their physical properties. In particular is the mismatch of their coefficients of thermal expansion with Ti alloy and PHSS having coefficient of thermal expansion $3.36 \times 10^{-8}/\text{K}$ and $1.08 \times 10^{-5}/\text{K}$, respectively, which results in large residual stress in the joints after processing.^[3] Diffusion bonding has proved to be a near net shape forming process for simultaneous joining and manufacturing of Ti alloy materials without gross macroscopic distortion and with minimum dimensional

tolerances, as Ti alloy exhibits both the superplasticity and diffusion bonding under the same conditions.^[4-6]

The literature reports that the intermetallic phases were formed at the diffusion interface of the transition joint consisting of Ti/Ti alloy and steel/stainless steel, which deteriorates the bond strength of the transition joints.^[7-19] In the case of diffusion bonding of dissimilar materials, an interlayer inserted between substrates is often necessary to prevent the formation of intermetallic compound and to reduce the residual stress in the joints.^[2,20] In an earlier investigation, the present authors improved the strength and ductility properties of diffusion-bonded joints between commercially pure titanium and 304 stainless steel using pure Ni as an intermediate material and achieved the tensile strength of the joint which was comparable with the strength of commercially pure titanium.^[21] The literature reports that a shear strength of ~148 MPa was obtained for diffusion-bonded Ti-6Al-4V and 304 stainless steel web joint when processing was carried out at 1123 K to 1153 K (850 °C to 880 °C) for 10 to 20 minutes under 10 to 15 MPa load using a 30- μm -thick pure Ni interlayer.^[22] However, direct bonding of these two dissimilar materials results in a lower bond shear strength of ~72 MPa.^[23] In an earlier investigation, Ti alloy to 17-4 PHSS joint was carried out by a brazing technique and a maximum shear strength of ~233 MPa had been achieved at 1123 K (850 °C) for 180 seconds using a 10- μm -thick (72Ag-28Cu in wt pct) braze alloy.^[2]

S. KUNDU, Assistant Professor, G. ANAND, Post-Graduate Student, and S. CHATTERJEE, Professor and Director of Research and Consultancy, are with the Department of Metallurgy and Materials Engineering, Bengal Engineering and Science University, Shibpur, Howrah 711103, West Bengal, India. Contact e-mail: skundu@metal.becs.ac.in, erskundu@yahoo.com

Manuscript submitted November 25, 2011.

Article published online November 30, 2012

The present paper reports the study on the diffusion bonding of Ti alloy and 17-4 PHSS using the 150 μm thickness Ni alloy interlayer in the temperature range of 1073 K to 1223 K (800 $^{\circ}\text{C}$ to 950 $^{\circ}\text{C}$) for 60 minutes under 5 MPa load. Also, the 17-4 PHSS without Ni alloy interlayer is included in the experiment for the purpose of comparison in terms of microstructural evolution, interfacial reaction, and mechanical properties of the diffusion-bonded joint.

II. EXPERIMENTAL PROCEDURES

A. Base Materials: Precipitation Hardening Stainless Steel, Ti Alloy, and Ni Alloy

17-4 PHSS and titanium alloy (TiA) were used in the form of a 40-mm-diameter rod in hot-rolled condition. The 150- μm -thick nickel alloy (NiA) interlayer was used as an intermediate material. The chemical compositions of base metals and NiA interlayer have been presented in Table I, while Table II provides the room temperature mechanical properties of base metals. The hot-rolled rods of the parent metals were machined to the dimensions 30 mm length and 16 mm diameter.

B. Surface Preparation

In all cases, the circular cross section of PHSS and TiA samples were prepared by a conventional grinding and polishing technique to obtain a surface roughness of ~ 0.5 to $0.6 \mu\text{m}$. The NiA foil of 150 μm thickness was used as an intermediate material and both the surfaces of the interlayer were polished following the standard metallurgical specimen preparation procedure. The bonding surfaces were cleaned in acetone and dried in air. The PHSS|TiA or PHSS|NiA|TiA assemblies were kept in contact in a fixture and were inserted in a vacuum chamber. The diffusion bonding was carried out in the temperature range of 1073 K to 1223 K (800 $^{\circ}\text{C}$ to 950 $^{\circ}\text{C}$) in steps of 298 K (25 $^{\circ}\text{C}$) for 60 minutes in $(2\text{--}5) \times 10^{-4}$ Pa vacuum. The compressive stress of 5 MPa was applied along the axial direction of the samples and the stress was measured at room temperature. The heating was done at the rate of 293 K min^{-1}

(20 $^{\circ}\text{C min}^{-1}$) at the time of processing and after the operation; the samples were allowed to cool in vacuum at a cooling rate of 273.02 K s^{-1} (0.2 $^{\circ}\text{C s}^{-1}$) up to 623 K (350 $^{\circ}\text{C}$) and then the samples were allowed to cool in air till room temperature.

C. Microstructural Characterizations

For metallographic examination, the bonded joints were sectioned transversely to the bond line, grounded, polished, and etched with a separate reagent for separate materials. The TiA and PHSS sides were etched with Kroll's reagent (6 mL HCl, 2 mL HF, and 92 mL H_2O) and Fay's reagent (40 mL HCl, 25 mL $\text{C}_2\text{H}_5\text{OH}$, 30 mL H_2O , and 5 gm CuCl_2), respectively. The NiA interlayer was etched by waterless Kalling reagent consisting of 5 gm CuCl_2 , 100 mL HCl, and 100 mL $\text{C}_2\text{H}_5\text{OH}$. Polished surfaces of bonded couples were examined in a scanning electron microscope (JSM-5510, JEOL) in backscattered mode (SEM-BSE) to obtain structural details in the diffusion interfaces. The composition of the chemical species in the reaction layers across their width was determined in weight percent by energy dispersive spectroscopy (EDS) (Thermo Electron Corporation-Noran System Six C10018) and the average of the same was determined by calculating the arithmetic mean. Using a Scanning Electron Microscope (SEM), individual phase width was measured from the cursor position. Five such readings were taken from different locations and an average of them was incorporated in the results. The presence of intermetallic phases on the fracture surfaces was confirmed by x-ray diffraction (Philips PW 1840) using a copper target. The scanning range of 20 to 80 deg with a step size of 0.01° ($= 2\theta$) was used during diffraction study. Fracture surfaces of bonded samples were observed in secondary electron mode of SEM (JSM-5510, JEOL) using energy dispersive spectroscopy (Thermo Electron Corporation-Noran System Six C10018) to reveal the nature and location of failure under loading.

D. Evaluation of Mechanical properties

Cylindrical tensile specimens were machined as per ASTM specification E8M-97 with a gauge diameter and length of 4 mm and 20 mm, respectively.^[24] The interface

Table I. Chemical Compositions of the Parent Materials (Wt Pct)

Alloy	C	Fe	Ti	Mn	Si	S	P	Cr	Ni	Cu	Al	V	O
Ti alloy	0.02	0.1	bal	–	–	–	–	–	–	–	6.1	3.9	0.12
PHSS	0.04	bal	–	0.52	0.33	0.011	0.03	16.4	4.1	3.12	–	–	–
Ni alloy	–	8.6	–	–	–	–	–	16.7	bal.	–	0.3	–	–

Table II. Mechanical Properties of the Base Metals at Room Temperature

Alloy	Shear Strength (MPa)	0.2 Pct Proof Stress (MPa)	Ultimate Tensile Strength (MPa)	Fracture Elongation (Pct)
Ti alloy	643.5	886.3	978.0	20
PHSS	716.3	993.2	1056.4	21

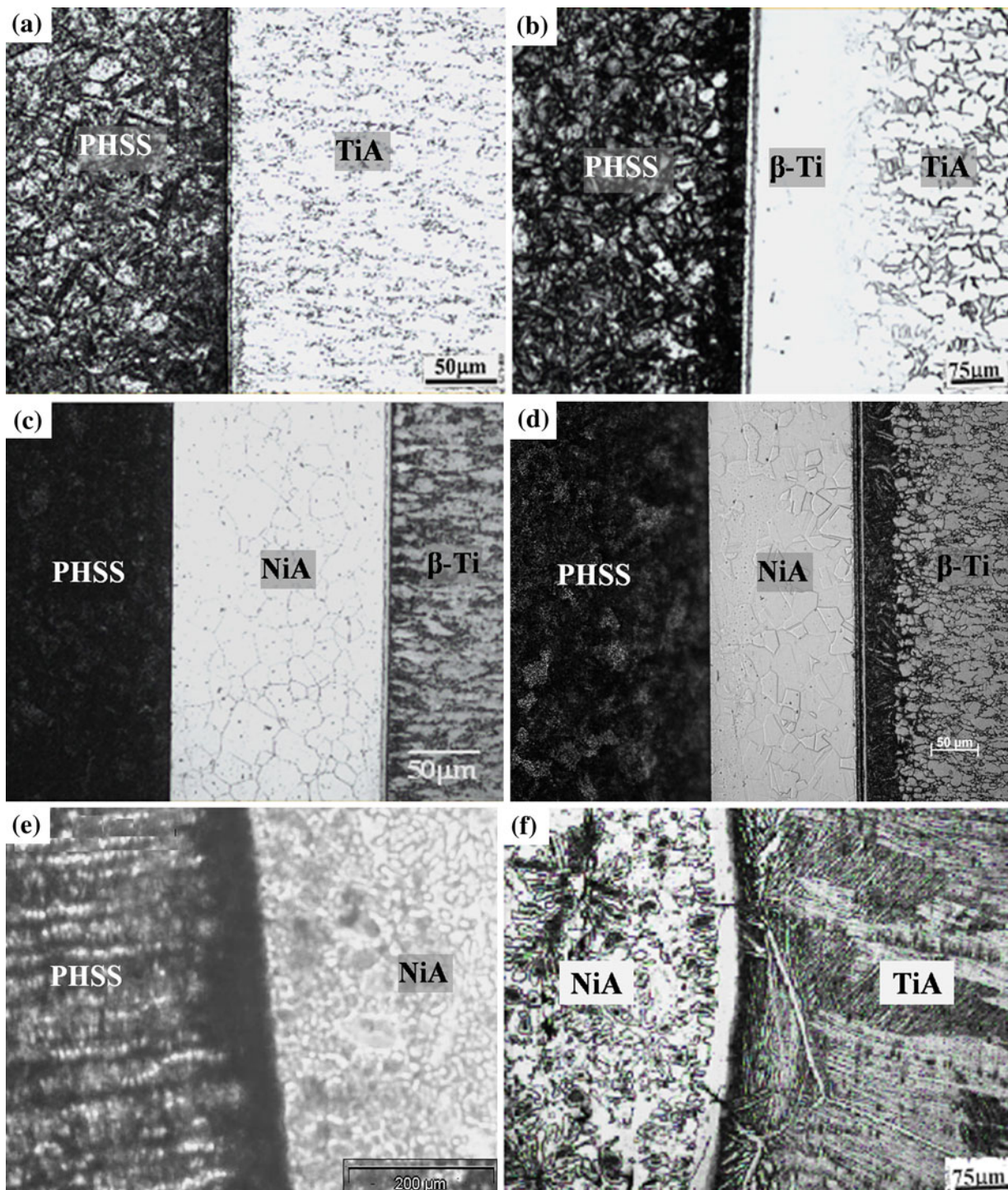


Fig. 1—Optical images of the diffusion-bonded joints of with and without intermediate material (a) PHSS/TiA at 1123 K (850 °C), (b) PHSS/TiA at 1223 K (950 °C), (c) PHSS/NiA/TiA at 1073 K (800 °C), (d) PHSS/NiA/TiA at 1148 K (875 °C), (e) PHSS/NiA/TiA at 1173 K (900 °C) at PHSS-NiA interface, (f) PHSS/NiA/TiA at 1173 K (900 °C) at NiA-TiA interface.

and interlayer were at the center of the gauge length of without and with interlayer diffusion-bonded joints, respectively. The tensile properties of the transition joints were evaluated in a universal testing machine (Instron 4204) at a crosshead speed of $8.33 \times 10^{-4} \text{ mm s}^{-1}$ at room temperature. Shear test specimens were machined to a diameter of 10 mm and shear strength of the bonded joint

was evaluated at room temperature using a screw tensile testing machine set at a crosshead speed of $8.33 \times 10^{-3} \text{ mm s}^{-1}$. Four samples were tested at each process parameter to check the reproducibility of results. The microhardness measurements on the polished bonded sample were carried out on a diamond micro-indenter using a 100 gf load with dwelling time of 15 seconds.

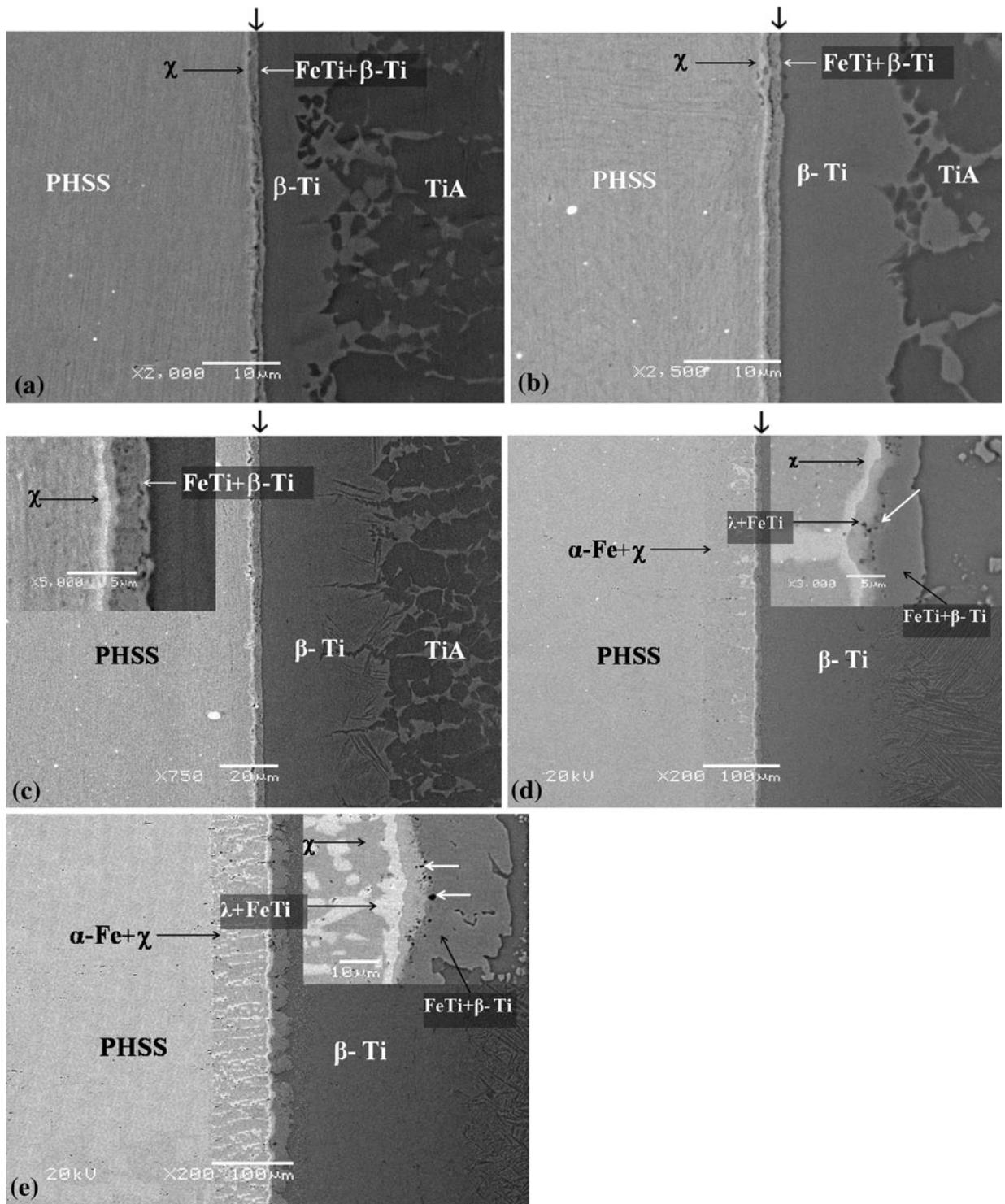


Fig. 2—Scanning Electron microscopy-backscatter electron images of PHSS/TiA diffusion-bonded joints processed for 60 min at (a) 1123 K (850 °C), (b) 1148 K (875 °C), (c) 1173 K (900 °C), (d) 1198 K (925 °C), (e) 1223 K (950 °C).

III. RESULTS AND DISCUSSION

A. Microstructural Characterization of the Diffusion Zone

Bonding temperature is one of the most important parameters in diffusion bonding as it strongly influences the characteristics of the bonded joints. The interface

microstructure, diffusion layer thickness, and phase composition of the reaction zone depend on the bonding temperature for a particular joining time.

1. Optical microstructure of diffusion-bonded joints

The optical micrograph of the diffusion-bonded joints with and without intermediate material is shown in

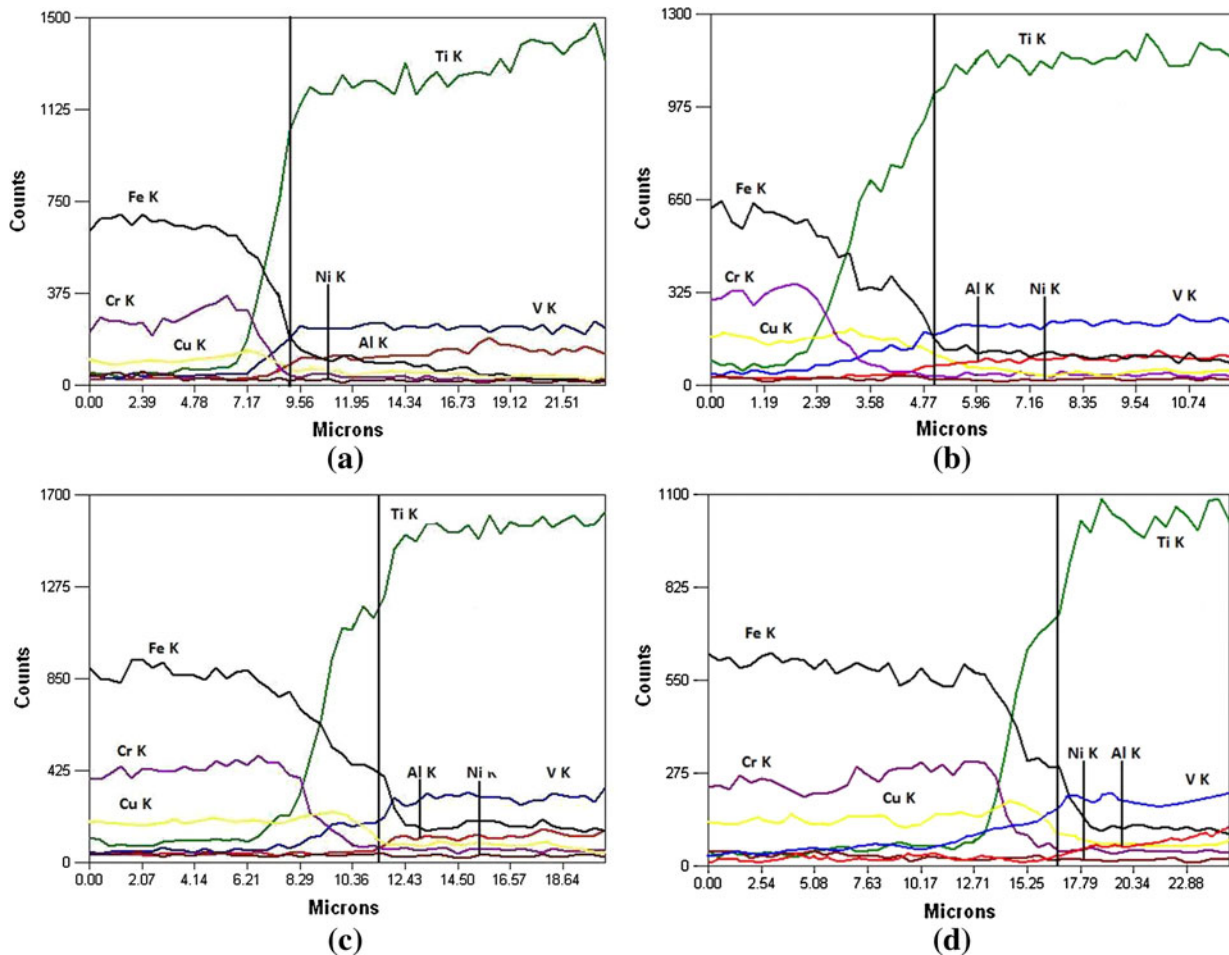


Fig. 3—EDS elemental line profile of PHSS/TiA diffusion-bonded joints processed for 60 min at (a) 1123 K (850 °C), (b) 1148 K (875 °C), (c) 1173 K (900 °C), (d) 1198 K (925 °C). (The black horizontal line corresponds to the vertical arrow as shown in Fig. 2, showing bond interface).

Figure 1. The diffusion zones are free from discontinuities and one interface (i.e., PHSS-TiA) for the directly bonded samples and two interfaces (i.e., PHSS-NiA and NiA-TiA) for the indirectly bonded samples (using interlayer) are clearly evident (Figure 1(a) through (f)). The extreme left side indicates the PHSS, while the right side shows the Ti alloy. At the PHSS-TiA interface for the directly bonded joints, the heavily etched band consisting of a layer of intermetallic phases is present (Figure 1(a) and (b)), while in the case of the indirectly bonded samples, the NiA-TiA interface (Figure 1(c) through (d), (f)) exhibits the layer of intermetallic phases as observed in the case of Figure 1(a) and (b). The PHSS-NiA interface for the indirectly bonded samples is planar in nature and a thin diffusion layer was revealed up to 1148 K (875 °C) (Figure 1(c) and (d)). Since Fe, Cr, and V are strong β -stabilizers of Ti, the migration of Fe, Ni, and Cr from PHSS to Ti alloy and the presence of V influence the retention of the high temperature bcc β -phase of Ti alloy at ambient temperature; hence, the bright area is designated as stabilized β -Ti (Figure 1(b)). The Widmanstatten morphology (the bright β -Ti phase is embedded in shaded α -Ti matrix) has been observed next to the bright phase due to a substantial quantity of

Fe, Cr, Ni, and V in this area, which promotes eutectoid transformation of Ti alloy.^[16,21–23]

Figures 1(e) and (f) show the optical micrograph for the PHSS-NiA and NiA-TiA sides, respectively, of the indirectly bonded sample at 1173 K (900 °C). Both of these figures clearly show the formation of reaction products in the interlayer, possibly due to the high bonding temperature.

2. SEM images of diffusion-bonded joints

The SEM-BSE images and EDS elemental line profiles of PHSS/TiA diffusion-bonded joints are shown in Figures 2 and 3, respectively. The bonding interface is resolved at higher magnifications. The bond line is clearly visible for all the bonded joints. It is observed that layerwise reaction products were formed near the diffusion interface. The chemical compositions of the reaction product formed in diffusion zone are given in Table III. The bright reaction layer of χ phase was observed at the PHSS side.^[25] A shaded reaction layer was found at the TiA side which is a phase mixture of FeTi + β -Ti. At 1173 K (900 °C) and above processing temperatures (Figure 2(c) through (e)), another light-shaded reaction layer has been found in between χ phase

Table III. EDS Chemical Analysis of the PHSS/TiA Bonded Joints at the Diffusion Interface (Wt Pct)

Phases	Fe	Cr	Ni	Cu	Ti	Al	V
α -Fe + χ	64.2-66.2 ± 0.51	23.2-27.5 ± 0.29	3.6-4.2 ± 0.31	1.1-1.3 ± 0.08	5.6-6.6 ± 0.21	—	—
χ phase	56.2-57.8 ± 0.43	22.4-23.7 ± 0.31	2.9-3.1 ± 0.15	0.8-1.1 ± 0.05	14.7-15.9 ± 0.21	0.03-0.3 ± 0.03	0.05-0.2 ± 0.01
FeTi + λ	51.2-54.3 ± 0.16	11.2-12.7 ± 0.23	2.1-2.4 ± 0.09	0.3-0.6 ± 0.05	28.9-29.7 ± 0.024	0.2-0.6 ± 0.04	0.2-0.4 ± 0.04
FeTi + β -Ti	38.7-40.2 ± 0.31	2.9-3.9 ± 0.13	2.2-2.4 ± 0.11	0.1-0.3 ± 0.06	51.6-54.3 ± 0.42	0.2-0.9 ± 0.03	0.2-0.6 ± 0.03

and FeTi + β -Ti phase mixture; the reaction layer is possibly the phase mixture of FeTi + λ . Another reaction layer of α -Fe + χ phase mixture was revealed at 1198 K (925 °C) and above bonding temperature (Figure 2(d) and (e)). The phase and phase mixture predicted from the EDS analysis are obtained by comparing the concentration of alloying elements with the ternary isotherm of Fe-Cr-Ti at 1073 K, 1123 K, 1173 K, and 1123 K (800 °C, 850 °C, 900 °C, 950 °C) and the effects of Ni, V, Al, and Cu are ignored as their concentrations are low enough to form any intermetallics in combination with Fe, Cr, and Ti in the present investigation.^[25] The χ phase is found to be Fe₁₇Cr₇Ti₅. As per the phase diagram, the concentration of Fe, Cr, and Ti in χ phase with complex cubic structure is given in Table III. The λ phase is found to be the phase mixture of Fe₂Ti and Cr₂Ti.^[11,25]

The FeTi + λ and α -Fe + χ phase mixture had not been observed in the PHSS-TiA side till 1173 K (900 °C) due to very low volume fraction. The light-shaded area in the TiA side for all bonded assemblies is the stabilized β -Ti.^[22] The width of the reaction products increases with the increase in bonding temperature which is shown in Figure 4.

The SEM-BSE micrographs and EDS elemental line profiles of the PHSS-NiA diffusion interface of the PHSS-NiA-TiA bonded samples are shown in Figures 5 and 6, respectively. At the PHSS-NiA interface, the diffusion zone is free from intermetallics up to a bonding temperature of 1148 K (875 °C) (Figure 5(a) and (b)), and composition along the bond interface changes abruptly for Fe and Ni. The EDS line profile clearly indicates that Cr concentrations are same at the both sides (Figure 6).

However, at 1173 K (900 °C) and above bonding temperature, the layerwise reaction products have been observed at the PHSS-NiA interface (Figure 5(c) and (d)). At a high temperature of bonding (i.e., 1173 K (900 °C) and above), the NiA interlayer cannot restrict the migration of Ti atoms to PHSS lattice and vice

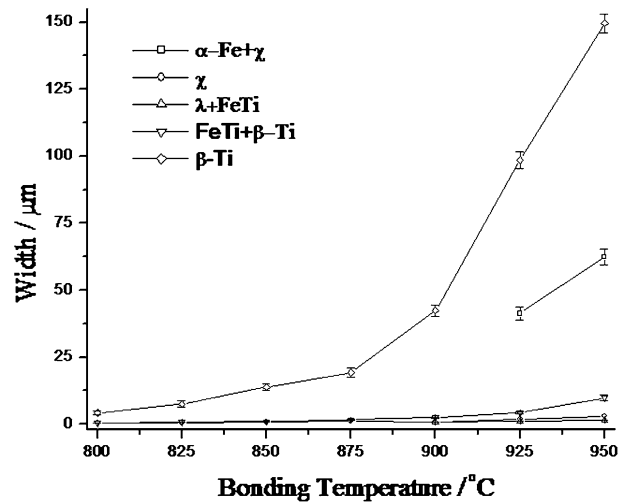


Fig. 4—Width of intermetallics formed at the interface of PHSS/TiA diffusion-bonded joints.

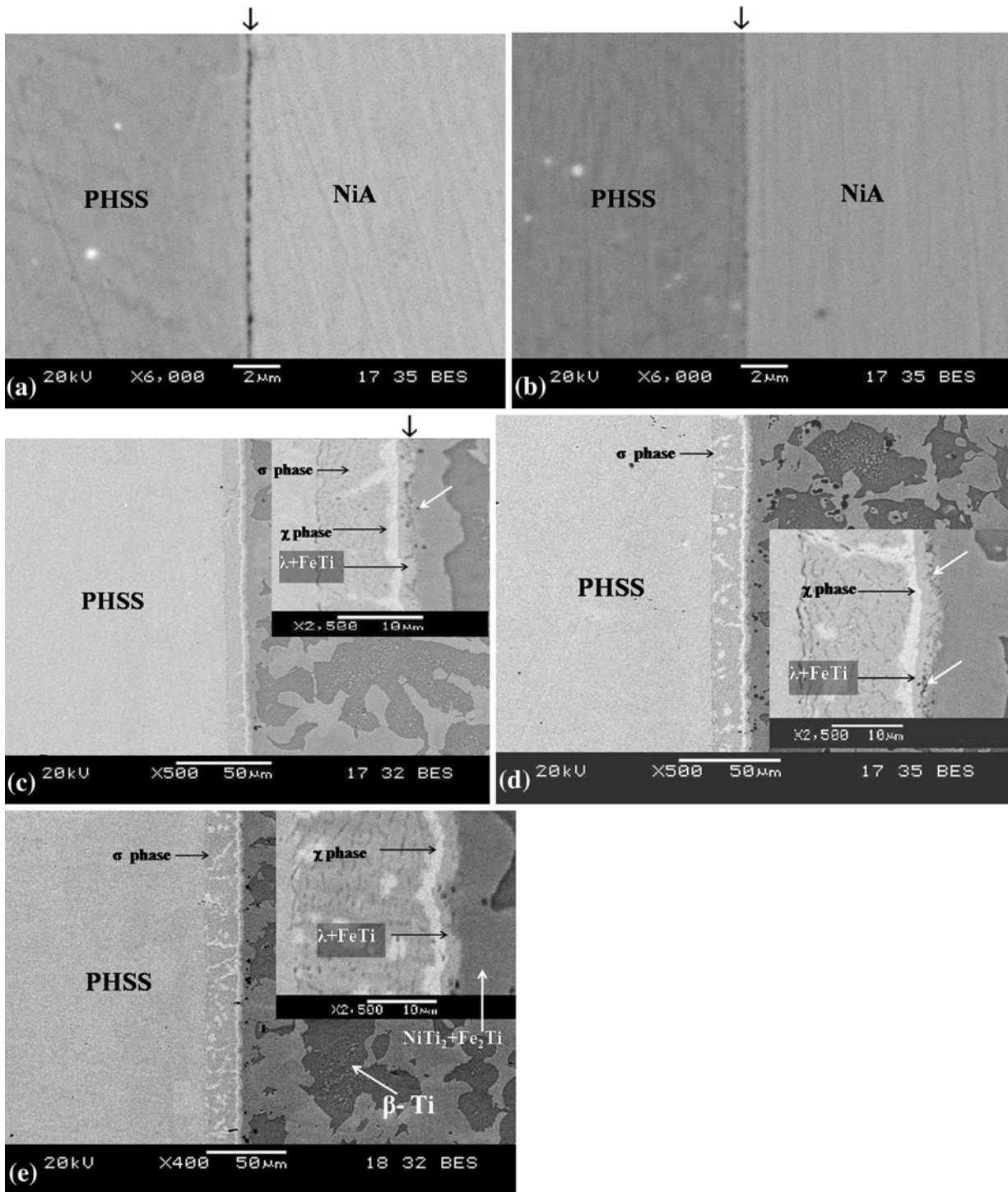


Fig. 5—SEM-BSE images of PHSS/NiA/TiA diffusion-bonded joints at PHSS-NiA interfaces processed for 60 min at (a) 1073 K (800 °C), (b) 1148 K (875 °C), (c) 1173 K (900 °C), (d) 1198 K (925 °C), (e) 1223 K (950 °C).

versa and thus the formation of Fe-Cr-Ti and Fe-Ti-type intermetallics occurs at the PHSS-NiA interface. The chemical compositions of the reaction products' analysis from EDS are given in Table IV. The wide-shaded reaction layer of σ phase was observed near the PHSS side (marked in Figure 5(c) through (e)). Close to the σ phase, the thin bright-shaded region is found to be the phase mixture of χ phase. Another reaction layer has

been observed next to the χ phase (marked in Figure 5(c) through (e)). This area is possibly the phase mixture of $\lambda + \text{Fe}_2\text{Ti}$. The concentration of different alloying elements present in the phase and phase mixture has been analyzed by EDS and the phase and phase mixture were determined with the help of ternary isotherm of Fe-Cr-Ti at 1173 K, 1198 K, and 1223 K (900 °C, 925 °C, 950 °C).^[25] The effects of Ni, Cu, Al,

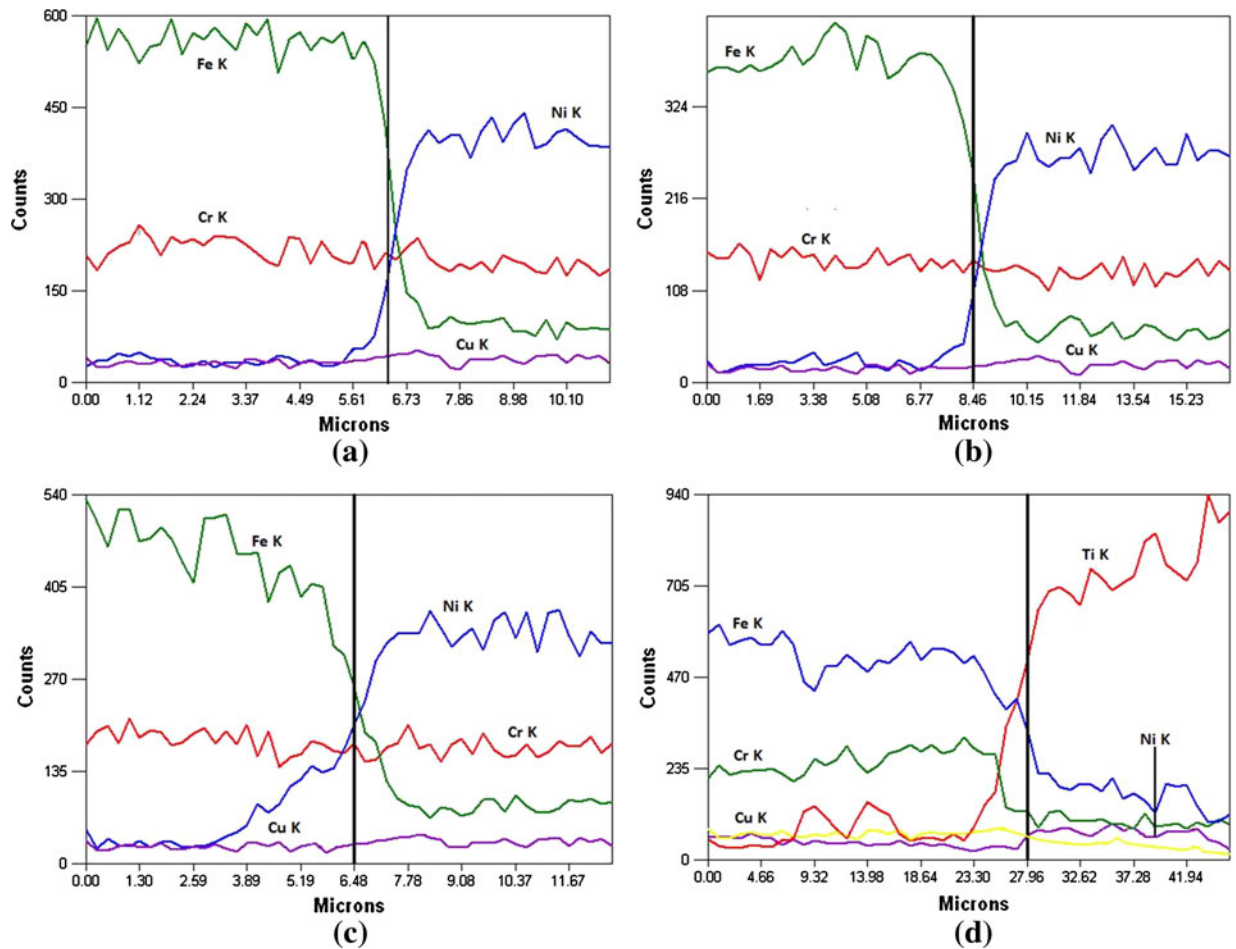


Fig. 6—EDS elemental line profile of PHSS|NiA|TiA diffusion-bonded joints processed for 60 min at PHSS-NiA interface at (a) 1073 K (800 °C), (b) 1123 K (850 °C), (c) 1148 K (875 °C), (d) 1173 K (900 °C) (The black horizontal line corresponds to the vertical arrow as shown in Fig. 5, showing bond interface).

and V are ignored as their concentration is low and not enough to form any intermetallics in combination with Fe, Cr, and Ti. The increase in joining temperature drives more numbers of atoms to migrate across the interface, which is responsible for the joining of the reaction layers.^[25–30] Figure 5(d) and (e) also show the presence of micro-voids at the interface of the phase mixture of $\lambda + \text{Fe}_2\text{Ti}$ and NiA, as marked by the arrow. The width of the reaction products increases with an increase in the bonding temperature and is presented in Figure 7.

It is important to note that at the NiA side (Figure 5(e)), the light-shaded and black regions along with irregular-shaped light-shaded particles were observed. The ternary isothermal section of the Fe-Ni-Ti diagram indicates that the light-shaded and irregular-shaped light-shaded particles are a phase mixture of $\text{NiTi}_2 + \text{Fe}_2\text{Ti}$,^[26] while, the black region is the $\beta\text{-Ti}$ phase.

The SEM micrographs and EDS line profiles of the NiA-TiA interface of indirectly diffusion-bonded samples are shown in Figures 8 and 9, respectively. It reveals that distinguishable diffusion layers have been observed in the diffusion interface and their chemical compositions are given in Table V. The bright-shaded layer is found to be the NiTi_2 phase near the TiA side (marked

as 3 in Figure 8(a) through (d)). Close to nickel alloy, the deep-shaded area is the Ni_3Ti phase (marked as 1 in Figure 8(a) through (d)).^[21,25] The bright irregular-shaped particle has been observed with the Ni_3Ti intermetallic, and their size increases with the increase in bonding temperatures. The composition of the bright particles is Fe (~5.1 to 5.5 wt pct), Ti (~13.9 to 4.6 wt pct), Cr (~35.2 to 5.8 wt pct), Ni (~45.7 to 46.3 wt pct), with small amounts of Al (~0.29 to 0.44 wt pct). So, these bright particles are presumably the phase of $\text{Fe}_5\text{Cr}_{35}\text{Ni}_{40}\text{Ti}_{15}$ (marked as the arrow in Figure 8(b) through (d)). Another reaction layer of NiTi has been observed in between Ni_3Ti and NiTi_2 (marked as 2 in Figure 8(a) through (d)). The widths of NiTi_2 , NiTi, and Ni_3Ti are increased with an increase in bonding temperature, which is shown in Figure 10.

However, at 1173 K (900 °C) and above bonding temperatures (Figure 8(e) and (f)), the absence of layer-wise reaction products at the NiA-TiA interface can be observed. At that interface, the light-shaded and black regions along with irregular-shaped light-shaded particles have been observed; the light-shaded region and irregular particles are presumably the $\text{NiTi}_2 + \text{Fe}_2\text{Ti}$ phase mixture, and the black region is $\beta\text{-Ti}$.^[26]

Table IV. EDS Chemical Analysis of the Reaction Layers Formed at PHSS-NiA Interface of PHSS/NiA/TiA Diffusion-Bonded Joints (Wt Pct)

Phases	Fe	Cr	Ni	Ti	Cu	Al	V
σ phase	55.1-56.1 \pm 0.60	37.9-38.4 \pm 0.35	3.1-3.5 \pm 0.36	2.6-2.9 \pm 0.16	0.5-1.1 \pm 0.06	—	—
χ phase	56.3-57.4 \pm 0.51	23.4-24.1 \pm 0.27	2.6-2.8 \pm 0.18	13.2-14.9 \pm 0.26	0.06-0.3 \pm 0.01	0.3-0.4 \pm 0.03	0.7-0.9 \pm 0.02
λ + Fe ₂ Ti	48.1-50.3 \pm 0.51	14.7-15.2 \pm 0.27	1.6-1.9 \pm 0.18	31.7-32.3 \pm 0.31	0.03-0.2 \pm 0.01	0.5-0.7 \pm 0.03	0.9-1.1 \pm 0.05
NiTi ₂ + Fe ₂ Ti	17.3-19.2 \pm 0.54	2.7-3.5 \pm 0.31	21.5-23.4 \pm 0.37	52.2-54.3 \pm 0.6	—	1.9-2.5 \pm 0.09	1.2-1.5 \pm 0.09
β -Ti	10.3-12.3 \pm 0.49	1.3-2.2 \pm 0.20	5.5-6.4 \pm 0.54	72.5-76.3 \pm 0.60	—	0.9-1.1 \pm 0.11	3.6-4.1 \pm 0.25

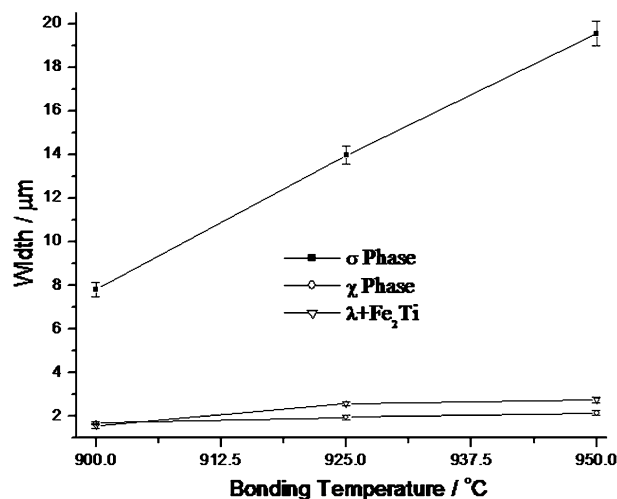


Fig. 7—Width of intermetallics formed at the PHSS-NiA interface of PHSS|NiA|TiA diffusion-bonded joints.

It is worth mentioning that at the PHSS/TiA joints' interface (marked as the arrow in Figure 2(d) and (e)) and the PHSS-NiA interface of PHSS/NiA/TiA joints (marked as the arrow in Figure 5(c) through (e)), dark irregular-shaped micro-voids have been observed at a higher bonding temperature. Their size increases with the increase in the bonding temperatures. The self-diffusion coefficient of α -Fe ($D_{\alpha\text{-Fe}} = 5 \times 10^{-15} \text{ m}^2 \text{ s}^{-1}$) and γ -Fe ($D_{\gamma\text{-Fe}} = 3 \times 10^{-17} \text{ m}^2 \text{ s}^{-1}$) is smaller than that of Ti ($D_{\text{Ti}} = 5.5 \times 10^{-14} \text{ m}^2 \text{ s}^{-1}$) at 1173 K (900 °C).^[26] So, the diffusion of titanium is faster than iron, which produces an imbalance in mass flow across the interface and generates voids. Hinotani *et al.*^[29] and Orhan *et al.*^[30] reported that the presence of such voids also occurs for the diffusion couples of titanium nickel and stainless steel-titanium alloy when processing was done at 973 K to 1073 K (700 °C to 800 °C) and 1073 K (800 °C), respectively.

3. X-ray diffraction pattern on the fracture surface

Figure 11 shows the x-ray diffraction patterns of the fracture surface of PHSS/TiA diffusion-bonded joints for different bonding temperature. The x-ray diffraction study indicates the occurrence of χ phase, Fe₂Ti, Cr₂Ti, FeTi, α -Ti, and β -Ti in the reaction zone. The λ phase being the solid solution of (Fe, Cr)₂Ti has been identified separately.^[28] The reaction region does not show the existence of any Cu-bearing intermetallics. The x-ray diffraction study exhibits the presence of σ phase at 1223 K (950 °C) (Figure 13(a)), but it could not be observed in SEM images due to low volume fraction. The σ phase is principally composed of Fe and Cr. The Cr enrichment occurs by uphill diffusion and during cooling, the chromium-enriched region transforms to the σ phase.^[28]

Figure 12 shows the x-ray diffraction patterns for fracture surfaces of the PHSS/NiA/TiA diffusion-bonded joints for different bonding temperatures. NiTi₂, NiTi, Ni₃Ti, Fe₅Cr₃₅Ni₄₀Ti₁₅, α -Ti, and β -Ti phases have been indicated in the reaction zone when the processing temperature is up to 1148 K (875 °C). However at 1173 K (900 °C) processing temperature, the formation of intermetallic compounds like NiTi₂,

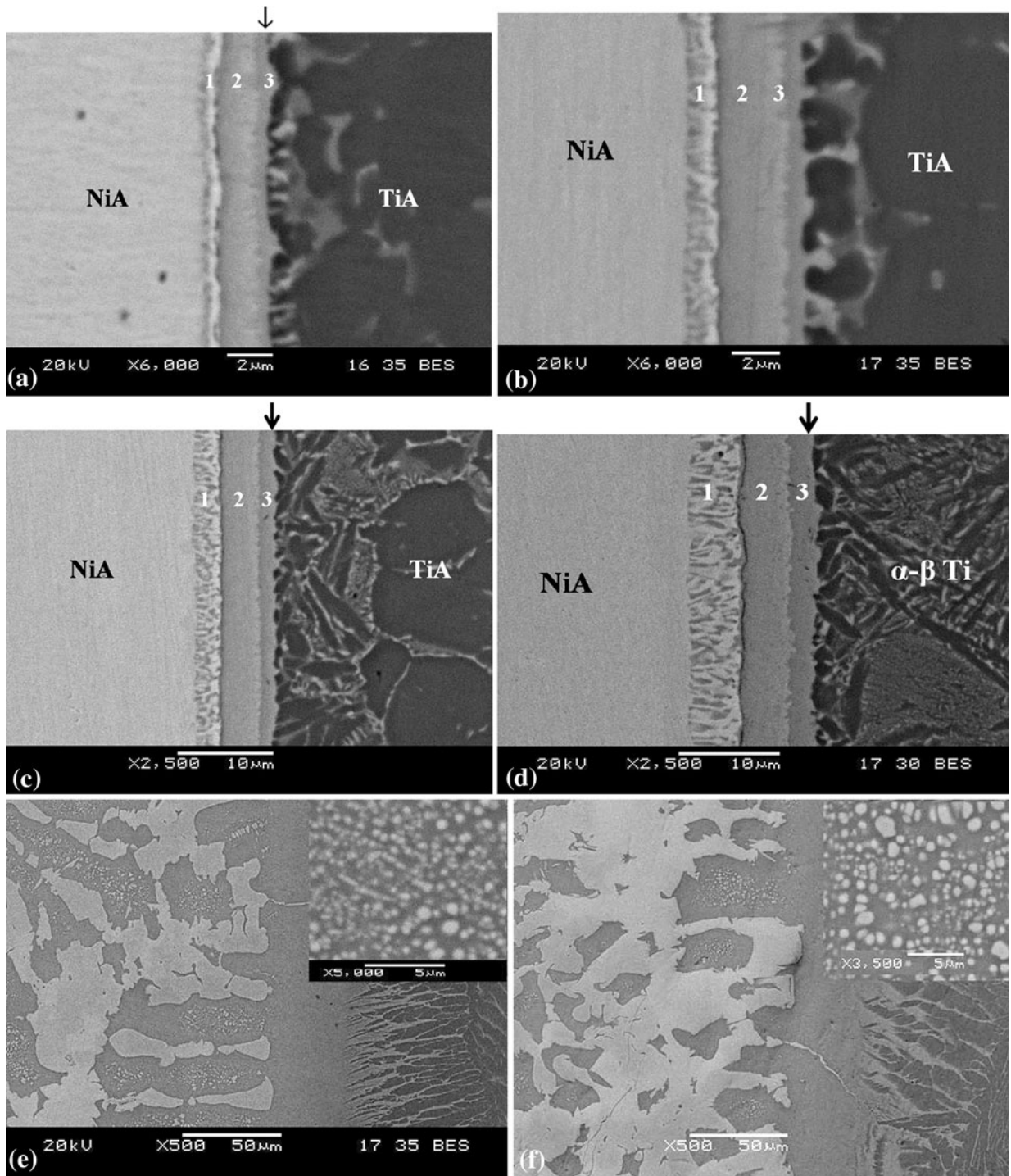


Fig. 8—SEM-BSE images of PHSS|NiA|TiA diffusion-bonded joints at NiA-TiA interfaces processed for 60 min at (a) 1073 K (800 °C), (b) 1098 K (825 °C), (c) 1123 K (850 °C), (d) 1148 K (875 °C), (e) 1173 K (900 °C), (f) 1223 K (950 °C). 1: Ni₃Ti, 2: NiTi, 3: NiTi₂.

Fe₂Ti, α -Ti and β -Ti has been observed. The SEM-BSE images shows that the σ phase, χ phase, and λ intermetallic compounds were observed at the PHSS-NiA interface; however, they are not revealed in the x-ray diffraction pattern due to the fact that the bonded samples were fractured through the NiTi₂ + Fe₂Ti and β -Ti region and the depth of x-ray diffraction was found to be not amenable for sub-surface detection.

B. Mechanical Properties of Diffusion-Bonded Joints

The room temperature mechanical properties of the PHSS/TiA diffusion-bonded joints with the change in bonding temperature are shown in Figure 13. It can be seen that the bond strength and elongation of the diffusion couple gradually increase with the increase in the bonding temperature and attain the maximum value

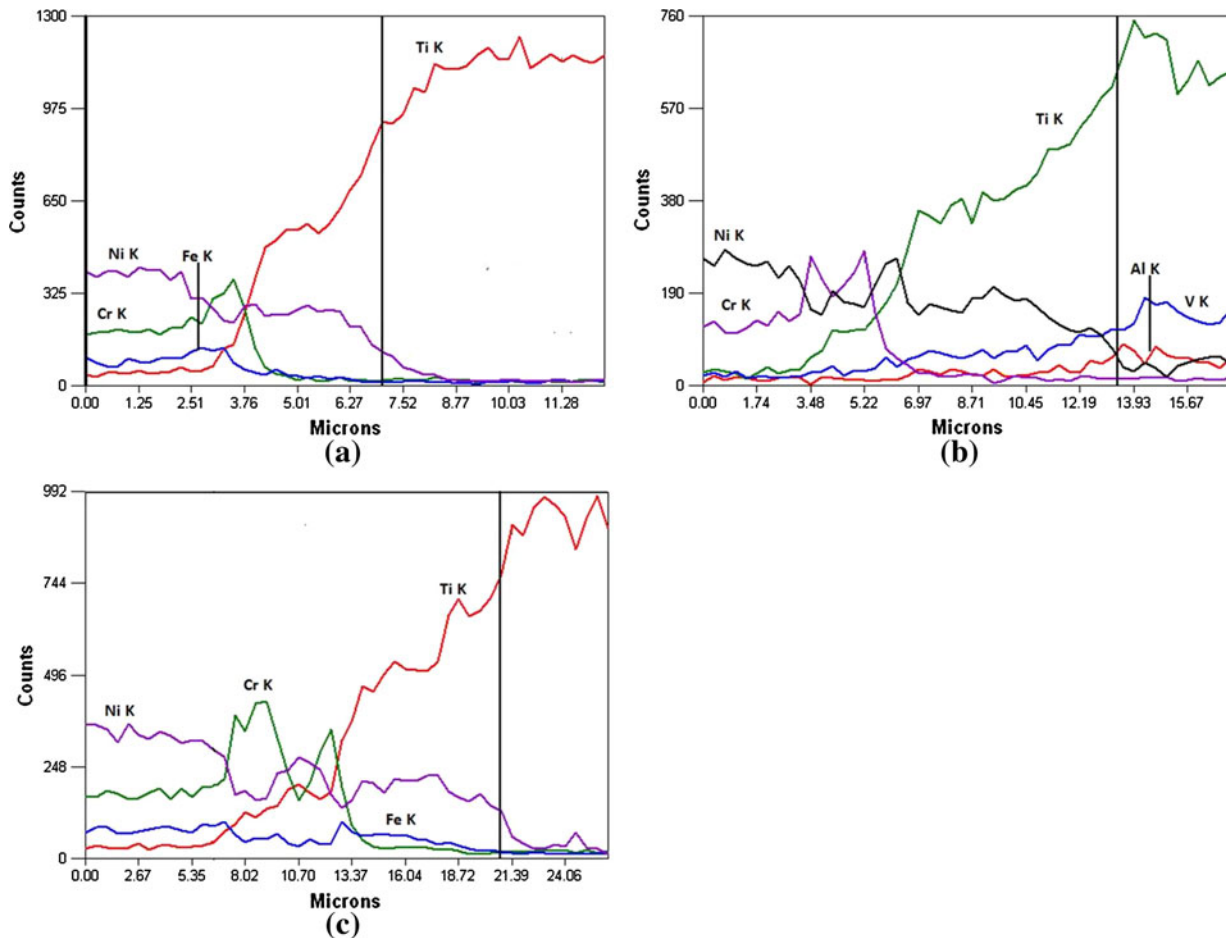


Fig. 9—EDS elemental line profile of PHSS/NiA/TiA diffusion-bonded joints processed for 60 min at the NiA-TiA interface at (a) 1073 K (800 °C), (b) 1123 K (850 °C), (c) 1148 K (875 °C). (The black horizontal line corresponds to the vertical arrow as shown in Figure 8, showing bond interface).

Table V. EDS chemical analysis of the reaction layers formed at NiA-TiA diffusion interface of PHSS/NiA/TiA diffusion-bonded joints (wt pct)

Phases	Fe	Ni	Ti	V	Al	Cr
NiTi ₂	0.9–1.1 ± 0.1	23.5–29.4 ± 0.26	68.1–74.5 ± 0.61	1.2–1.3 ± 0.1	1.5–1.7 ± 0.11	–
NiTi	2.5–3.5 ± 0.12	46.3–47.2 ± 0.31	45.4–46.5 ± 0.26	0.6–0.8 ± 0.06	1.1–1.3 ± 0.09	0.5–1.1 ± 0.09
Ni ₃ Ti	3.5–4.2 ± 0.11	69.5–72.2 ± 0.34	23.2–25.1 ± 0.26	–	0.5–0.7 ± 0.06	1.1–1.4 ± 0.05

at 1173 K (900 °C). At lower bonding temperatures, bond strength (both tensile and Shear strength) and elongation are low due to the incomplete coalescence of mating surfaces. The migration of atoms from titanium alloy to stainless steel and vice versa is very low and the yield strength of base materials is higher at a lower joining temperature as compared to a higher joining temperature.^[31] This leads to minimum thermal excitation and the extent of diffusion of alloying elements is limited. At the processing temperature of 1173 K (900 °C), bond strength is higher due to the plastic collapse of the asperities at the mating surface leading to the intimate contact, which overcompensates the embrittlement phenomena due to intermetallic phases, leading to increased bond strength and elongation.

With the rise in bonding temperature to 1198 K (925 °C) and above, the width of the intermetallic compounds increases (Figure 4) and the embrittlement effect overcompensates the effect due to the better plastic collapse of the mating surfaces. So, the bond strength and elongation gradually drop and attain the lowest value at 1223 K (950 °C) bonding temperature (bond tensile, shear strength, and elongation being ~312.6 MPa, 239.2 MPa, and 3.3 pct, respectively). It is also noticeable that at a higher temperature, the voids' size increases as compared with a lower bonding temperature, which also affects the bond strength.

The room temperature mechanical properties of the PHSS/NiA/TiA diffusion-bonded joints with the change in bonding temperature are shown in Figure 14. It can

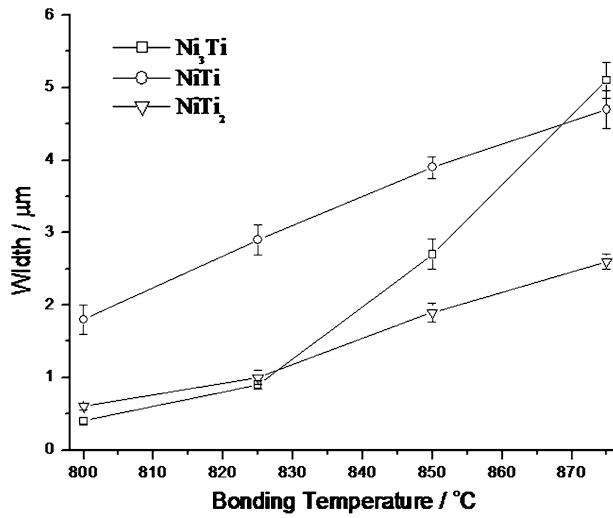


Fig. 10—Width of intermetallics formed at the NiA-TiA interface of PHSS|NiA|TiA diffusion-bonded joints.

be seen that bond strength and elongation increase with the increase in bonding temperature up to 1148 K (875 °C) and gradually fall with the increase in the bonding temperature. The bond strength increases with the increase in the bonding temperature due to the plastic collapse of the mating surface asperities leading to intimate contact, which overcompensates the embrittlement phenomena due to the intermetallic phases. So, bond strength increases. Maximum tensile strength of ~523.6 MPa, shear strength of ~389.6 MPa, and elongation of 6.3 pct have been achieved at 1148 K (875 °C) due to increased contact area between the mating surfaces, and it also promotes the inter-diffusion of alloying elements.

At 1173 K (900 °C) and above bonding temperature, the bond strength and elongation gradually decrease because the nickel alloy interlayer cannot block the diffusion of stainless steel to the TiA side and TiA to the PHSS side. So, Fe-Ti and Fe-Cr-Ti base intermetallics phase and phase mixture were formed at the PHSS-NiA

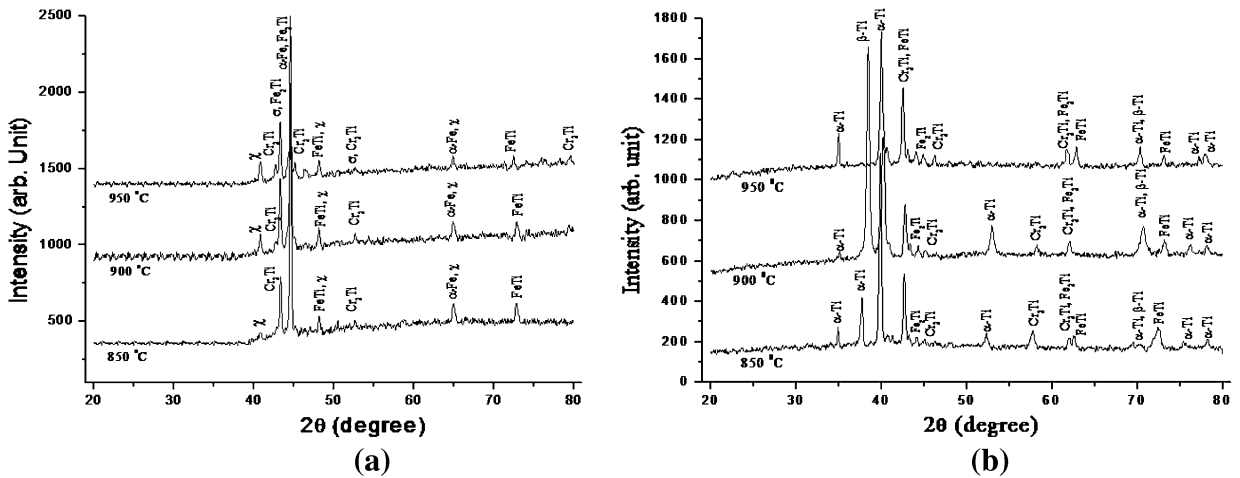


Fig. 11—X-ray diffraction patterns of the shear fracture surfaces of PHSS/TiA diffusion-bonded joints processed for 60 min at different temperatures at (a) PHSS side, (b) TiA side.

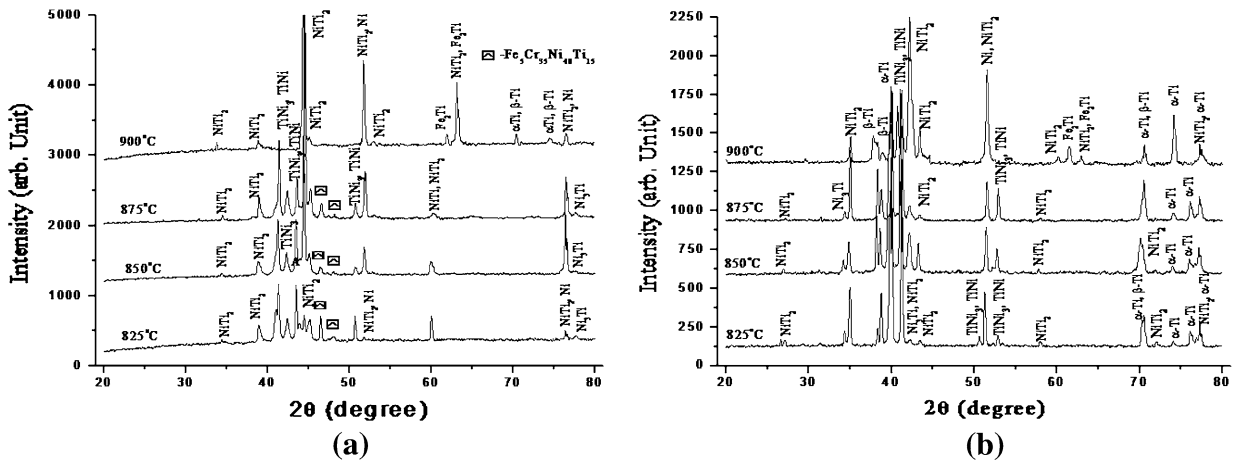


Fig. 12—X-ray diffraction patterns of the shear fracture surfaces of PHSS/NiA/TiA diffusion-bonded joints processed for 60 min at different temperatures at (a) PHSS side, (b) TiA side.

interface and the composite mixture of $\text{NiTi}_2 + \text{Fe}_2\text{Ti}$ and $\beta\text{-Ti}$ phase has covered the full nickel alloy interlayer. At these temperatures, the micro-voids have been observed in the SEM images (marked by the arrow in Figure 5(d) and (e)); hence, the discontinuities after

processing temperature of 1173 K (900 °C) presumably play a vital role in lowering the bond strength.

The maximum tensile strength of ~477 MPa and shear strength of ~356.9 MPa along with ~4.2 pct elongation were achieved for PHSS/TiA diffusion-bonded joint when

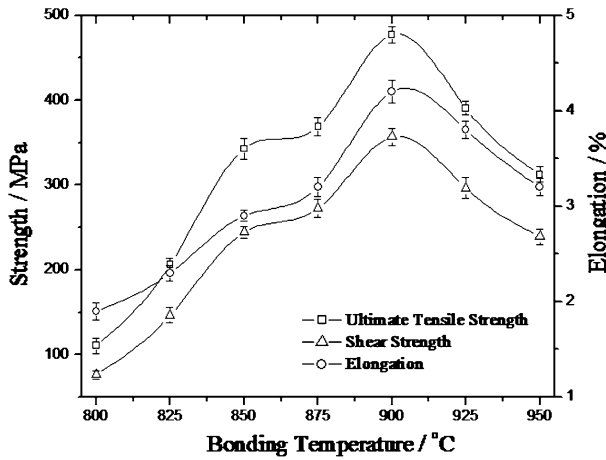


Fig. 13—Mechanical properties of the PHSS/TiA diffusion-bonded joints processed for 60 min.

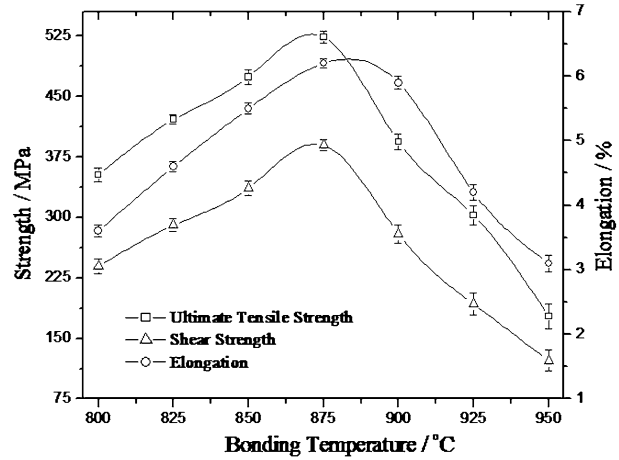


Fig. 14—Mechanical properties of the PHSS/NiA/TiA diffusion-bonded joints processed for 60 min.

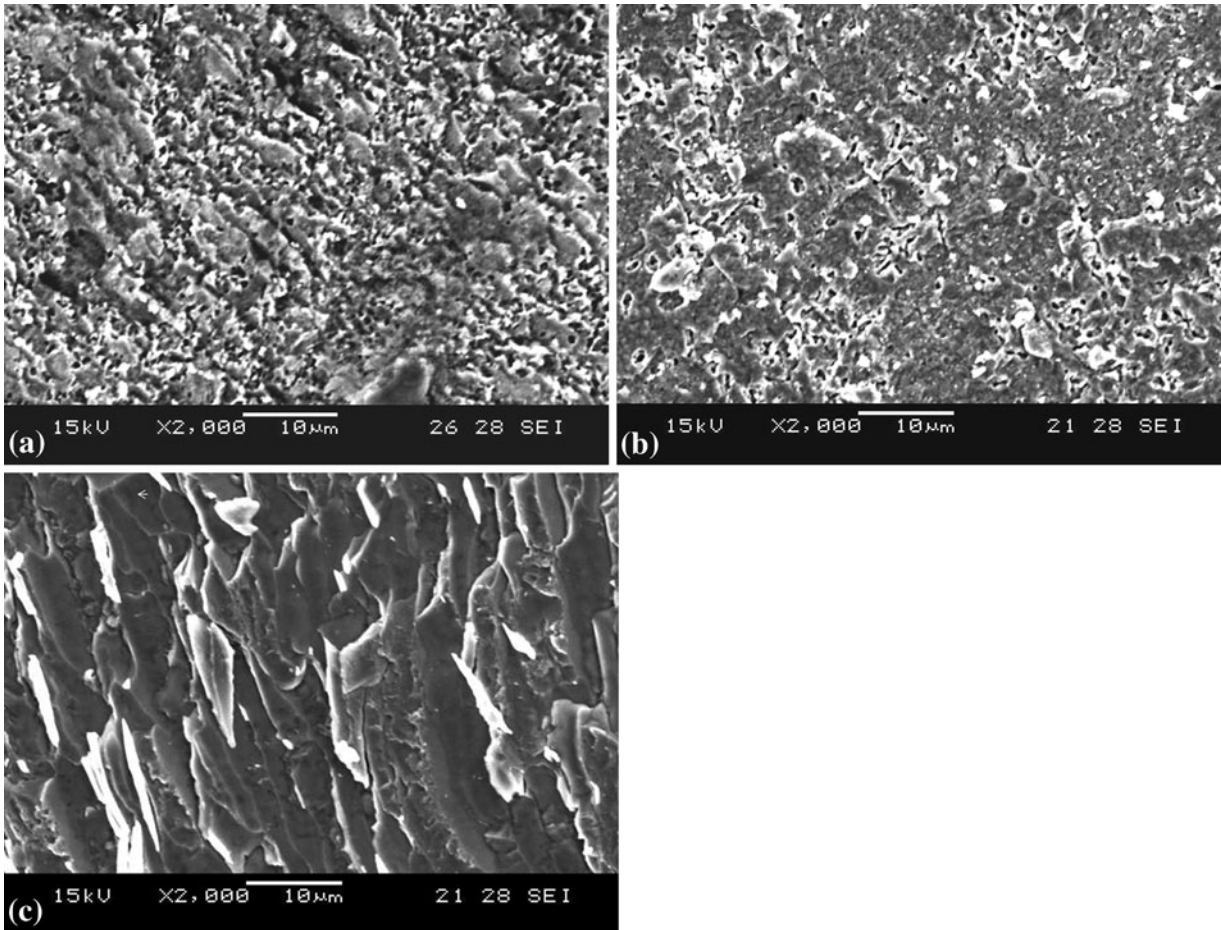


Fig. 15—Fracture surfaces of PHSS/TiA diffusion-bonded joints at TiA side processed at (a) 1073 K (800 °C), (b) 1123 K (850 °C), (c) 1198 K (925 °C).

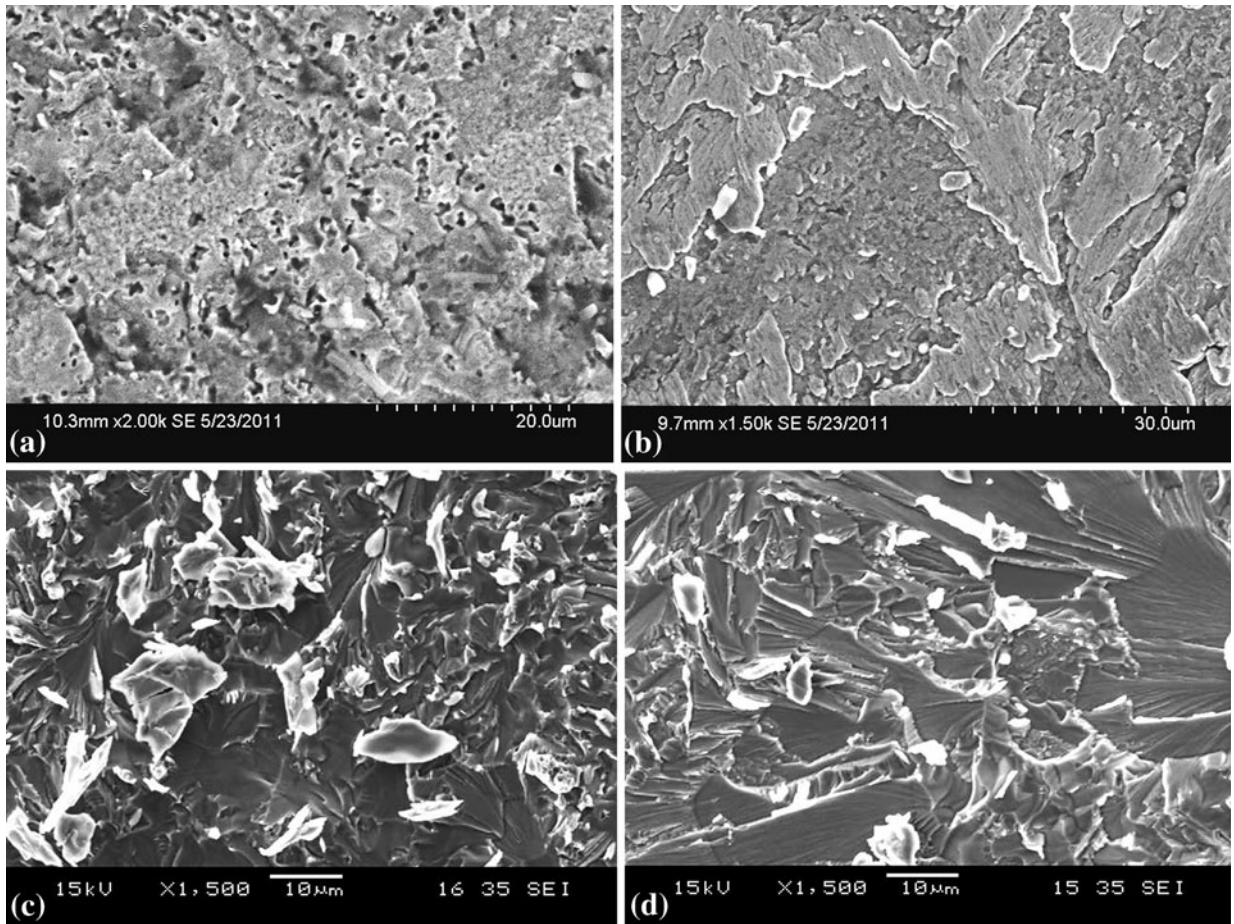


Fig. 16—Fracture surfaces of PHSS/NiA/TiA diffusion-bonded joints at TiA side processed at (a) 1098 K (825 °C), (b) 1148 K (875 °C), (c) 1173 K (900 °C), (d) 1198 K (925 °C).

processed at 1173 K (900 °C). However, when NiA was used as an interlayer in the same materials, the bond tensile and shear strengths increase to ~523.6 MPa and ~389.6 MPa, respectively, along with 6.2 pct elongation when bonding was processed at 1148 K (875 °C). The strength of the joints using the nickel alloy interlayer is higher as compared to that of the joints without interlayer due to the formation of Fe-Ti and Fe-Cr-Ti base intermetallics at their interface. It is observed that Fe-Ti and Fe-Cr-Ti base intermetallics are more brittle as compared to Ni-Ti base intermetallics. He *et al.*^[22] reported that Fe-Ti and Fe-Cr-Ti base intermetallics are more pernicious than Ni-Ti intermetallics in deteriorating the bond quality of the bonded joints.

C. Fracture Morphology of the Bonded Samples

The fracture morphology of the PHSS/TiA bonded assemblies is shown in Figure 15. At lower bonding temperatures, the fracture surfaces are basically featureless (Figure 15(a)). The dark area indicates the presence of voids and these irregular-shaped voids are generated presumably due to the insufficient elemental diffusion and lack of coalescence of the mating surfaces and encouraging the failure under load. The dark voids reduce with the increase in bonding temperature

(Figure 15(b)). However, for higher bonding temperature, the fracture surface (Figure 15(c)) clearly indicates the brittle nature of the transition joint by the presence of cleavage planes with different alignments. The shaded and bright regions have been noticed in the fracture surface. Both the shaded matrix and the bright line contain Ti (51.6 to 56.3 wt pct), Fe (36.7 to 40.2 wt pct), Cr (2.9 to 3.9 wt pct), Ni(2.1 to 2.6 wt pct), Al(0.07 to 0.09 wt pct), V(-0.02 to 0.03 wt pct), and Cu(bal.). The comparison of composition from Table III indicates that this area is presumably the FeTi + β -Ti phase mixture. So, the fracture in the directly bonded sample took place at the TiA side along the gauge length.

The fracture morphology of the PHSS-NiA-TiA bonded assemblies is shown in Figure 16. The fracture surface for a lower bonding temperature (Figure 16(a) and (b)) is basically featureless. The voids are present, as observed in the case of direct diffusion-bonded joints. Fracture surfaces for a higher bonding temperature (Figure 16(c) and (d)) clearly indicate the brittle nature of the transition joints by the presence of the cleavage planes with different alignments. The river pattern differs from grain to grain and the size of grain of river patterns increases with the increase in the bonding temperature. The shaded matrix and bright lines of the river pattern have been noticed in the fracture. The

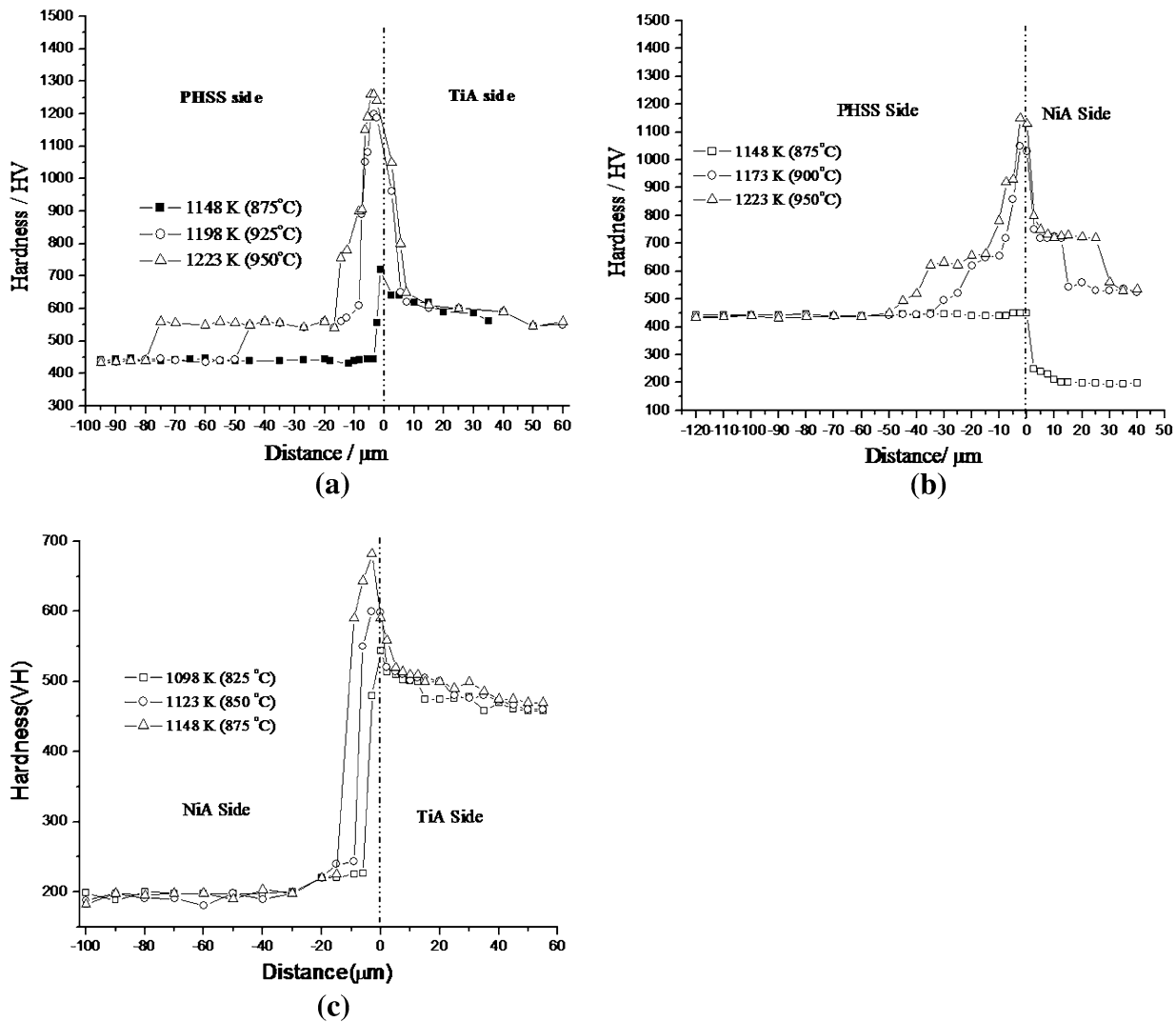


Fig. 17—Microhardness along the bond interfaces of (a) PHSS/TiA joints, (b) PHSS/NiA/TiA joints of PHSS-NiA interface, (c) PHSS/NiA/TiA joints of NiA-TiA interface.

shaded and bright regions are the NiTi_2 phase with compositions given in Table V. However, at 1173 K (900 °C) and above bonding temperature, these shaded and bright areas are $\text{NiTi}_2 + \text{Fe}_2\text{Ti}$ phase mixture. So, the fracture in the indirectly bonded sample took place at the NiA-TiA side along the gauge length.

D. Microhardness Analysis of the Bonded Joints

The microhardness measurement at the bond interface of the PHSS-TiA bonded joints at various temperatures are shown in Figure 17(a). It can be seen that the hardness of the interface is higher than that of the base material due to the presence of intermetallic phases at the bond interface. The microhardness values of the bond interface increase with the increase in bonding temperature due to the increase in volume fraction of brittle intermetallics at the interface.^[16,32] The maximum hardness value of $\sim 1260 \pm 20$ HV has been obtained at the interface region.

At the PHSS-NiA-TiA bonded joints, the microhardness measurement of the interfaces is shown in

Figure 17(b) and (c). At the PHSS-NiA interface (Figure 17(b)), the hardness value exhibited marginal change with respect to that of the base materials, when bonding was processed up to 1148 K (875 °C). However, at 1173 K (900 °C) and above, microhardness values increase due to the presence of brittle intermetallics at the above interface. The higher microhardness value is $\sim 1150 \pm 24$ HV at 1223 K (950 °C) at the same interface. However, at the NiA-TiA interface (Figure 17(c)), the high hardness in comparison with base metals is due to the formation of Ni-Ti-based intermetallics and hardness values increase with increasing bonding temperature. The maximum hardness value reaches $\sim 682 \pm 14$ HV at the interface.

IV. CONCLUSIONS

The microstructural evolution and mechanical properties of the diffusion-bonded joints of Ti alloy and 17-4 PHSS with and without NiA interlayer were evaluated

in this study. The important conclusions from the present investigation may be summarized as given below:

1. In the direct diffusion-bonded joints between PHSS and TiA, the layerwise χ , FeTi + β -Ti phase mixture were observed at the bond interface when the joint was processed up to 1173 K (900 °C); however, at 1198 K (925 °C) and above bonding temperatures, the layerwise α -Fe + χ , χ , FeTi + λ , FeTi + β -Ti phase mixture were observed.
2. When the 150 μm nickel alloy was used as an interlayer, the diffusion of Fe to TiA and Ti, V, Al to PHSS was completely restricted when bonding was carried out up to 1148 K (875 °C). However, at higher joining temperature, nickel alloy interlayer cannot block the diffusion of TiA to PHSS and σ phase, χ phase, and λ + Fe₂Ti phases were formed at the PHSS-NiA interface. Layerwise Ni₃Ti, NiTi, and NiTi₂ phases were formed and the irregular-shaped particles of Fe₅Cr₃₅Ni₄₀Ti₁₅ have been observed within the Ni₃Ti layer at the NiA-TiA interface up to 1148 K (875 °C) bonding temperature. However, their presence has not been observed at 1173 K (900 °C) and above bonding temperatures. Between NiA and TiA, β -Ti exists as discrete islands in the matrix of NiTi₂ + Fe₂Ti at the same bonding temperatures.
3. The maximum tensile strength of ~477 MPa and shear strength of ~356.9 MPa along with ~4.2 pct elongation were achieved for diffusion-bonded joints without interlayer when processed at 1173 K (900 °C). However, when NiA was used as an interlayer in the same materials, the bond tensile and shear strengths increase to ~523.6 MPa and ~389.6 MPa, respectively, along with 6.2 pct elongation when bonding was processed at 1148 K (875 °C).

REFERENCES

1. R.K. Shiue, S.K. Wu, C.H. Chan, and C.S. Huang: *Metall. Mater. Trans. A*, 2006, vol. 37A, pp. 2207–17.
2. R.K. Shiue, S.K. Wu, and J.Y. Shiue: *Mater. Sci. Eng., A*, 2008, vol. 488, pp. 186–94.
3. ASM: *ASM Metals Handbook*, 10th ed., ASM international, Metals Park, OH, 1990.
4. O. Torun, A. Karabulut, B. Baksan, and I. Çelikyürek: *Mater. Des.*, 2008, vol. 29, pp. 2043–46.
5. G. Can and M. Kocak: *Int. Mater. Rev.*, 1998, vol. 43, pp. 1–44.
6. A. Fuji, K. Ameyama, and T.H. North: *J. Mater. Sci.*, 1996, vol. 31, pp. 819–27.
7. S. Kundu, S. Chatterjee, D. Olson, and B. Mishra: *Metall. Mater. Trans. A*, 2008, vol. 39A, pp. 2106–14.
8. A. Chang and J. Zhangpeng: *J. Less Common Met.*, 1990, vol. 162, pp. 315–22.
9. X.J. Yuan, G.M. Sheng, B. Qin, W.Z. Huang, and B. Zhou: *Mater. Charact.*, 2008, vol. 59, pp. 930–36.
10. S. Kundu and S. Chatterjee: *Mater. Sci. Eng., A*, 2008, vol. 480, pp. 316–22.
11. B. Aleman, I. Gutiérrez, and J.J. Urcola: *Scripta Mater.*, 1997, vol. 36, pp. 509–15.
12. M. Eroglu, T.I. Khan, and N. Orhan: *Mater. Sci. Technol.*, 2002, vol. 18, pp. 68–72.
13. B. Kurt, N. Orhan, and M. Kaya: *Mater. Sci. Technol.*, 2009, vol. 25, pp. 556–60.
14. M. Ferrante and E.V. Pigoretti: *J. Mater. Sci.*, 2002, vol. 37, pp. 2825–33.
15. C.C. Liu, C.L. Ou, and R.K. Shiue: *J. Mater. Sci.*, 2002, vol. 37, pp. 2225–35.
16. N. Orhan, T.I. Khan, and M. Eroglu: *Scripta Mater.*, 2001, vol. 45, pp. 441–46.
17. G.M. Sheng, J.W. Huang, B. Qin, B. Zhou, and S.Y. Qiu: *J. Mater. Sci.*, 2005, vol. 40, pp. 6385–90.
18. B. Kurt, N. Orhan, E. Evin, and A. Çalik: *Mater. Lett.*, 2007, vol. 61, pp. 1747–50.
19. B. Qin, G.M. Sheng, J.W. Huang, B. Zhou, S.Y. Qiu, and C. Li: *Mater. Charact.*, 2006, vol. 56, pp. 32–38.
20. A.S. Ramos, M.T. Vieira, J. Morgiel, J. Grzonka, S. Simões, and M.F. Vieira: *J. Alloys Compd.*, 2009, vol. 484, pp. 335–40.
21. S. Kundu, S. Chatterjee, D. Olson, and B. Mishra: *Metall. Mater. Trans. A*, 2007, vol. 38A, pp. 2053–60.
22. P. He, J. Zhang, R. Zhou, and X. Li: *Mater. Charact.*, 1999, vol. 43, pp. 287–92.
23. P. He, J.H. Zhang, and X.Q. Li: *Mater. Sci. Technol.*, 2001, vol. 17, pp. 1158–62.
24. ASTM: *Annual Book of ASTM Standards*, ASTM, Philadelphia, 1997, vol. 3, pp. 87–89.
25. P. Villars, A. Prince, and H. Okamoto: *Handbook of Ternary Phase Alloys*, ASM International, Materials Park, OH, 1995, vol. 7.
26. V. Raghavan: *J. Phase Equilib. Diffus.*, 2010, vol. 31, pp. 186–89.
27. T.B. Massalski: *Binary Alloy Phase Diagrams*, 2nd ed., ASM International, Materials Park, OH, 1996, p. 1783.
28. B. Aleman, I. Gutiérrez, and J.J. Urcola: *Mater. Sci. Technol.*, 1993, vol. 9, pp. 633–41.
29. S. Hinotani and Y. Ohmori: *Trans. Jpn. Inst. Met.*, 1988, vol. 29, pp. 116–24.
30. N. Orhan, M. Aksoy, and M. Eroglu: *Mater. Sci. Eng., A*, 1999, vol. 271, pp. 458–68.
31. G.E. Dieter: *Mechanical Metallurgy*, SI Metric ed., McGraw-Hill Book Company, London, 1998.
32. J.H. Li and R.Y. Lin: *Mater. Sci. Eng.*, 2004, vol. A381, pp. 39–50.